Supplemental Information:

Content:

- Figure S1. Accessibility of the *L. interrogans* proteome by LC-MS analysis.
- Figure S2. Functional annotation of the identified proteins.
- Figure S3. Distribution of MS1-feature intensities.
- Figure S4. Comparison of the DDA- and directed (INL) LC-MS/MS strategy employed.
- Figure S5. Performance of the directed MS-workflow using different LC-MS/MS platforms.
- Figure S6. Reproducibility of label-free quantification of the *L. interrogans* proteome.
- Figure S7. Correlation of the estimated protein abundances (in copies/cell) with a recently published study.
- Figure S8. Determination of cellular protein concentrations.
- Figure S9. Significant protein changes in control samples after 24 and 48 hours without any treatment.
- Figure S10. Impact of relative (in fold) and absolute (in copies/cell) protein level changes on the *L. interrogans* proteome.
- Figure S11. Proteins of the bacterial chemotaxis pathway covered in cluster S-5 as assigned by DAVID using the KEGG database.
- Figure S12. Proteins of the TCA cycle covered in cluster S-5 as assigned by DAVID using the KEGG database.
- Figure S13. Proteins of the oxidative phosphorylation pathway covered in cluster S-5 as assigned by DAVID using the KEGG database.
- Table SI. Protein abundance levels determined by stable isotope dilution LC-MS.
- Table SII. Identified features during discovery phase (see xls-file).
- Table SIII. Identified proteotypic peptides (PTPs) during discovery phase (see xls-file).
- Table SIV. Identified proteins during discovery phase (see xls-file).
- Table SV. Monitored proteins during scoring phase (all treatments, see xls-file).

Figure S1:

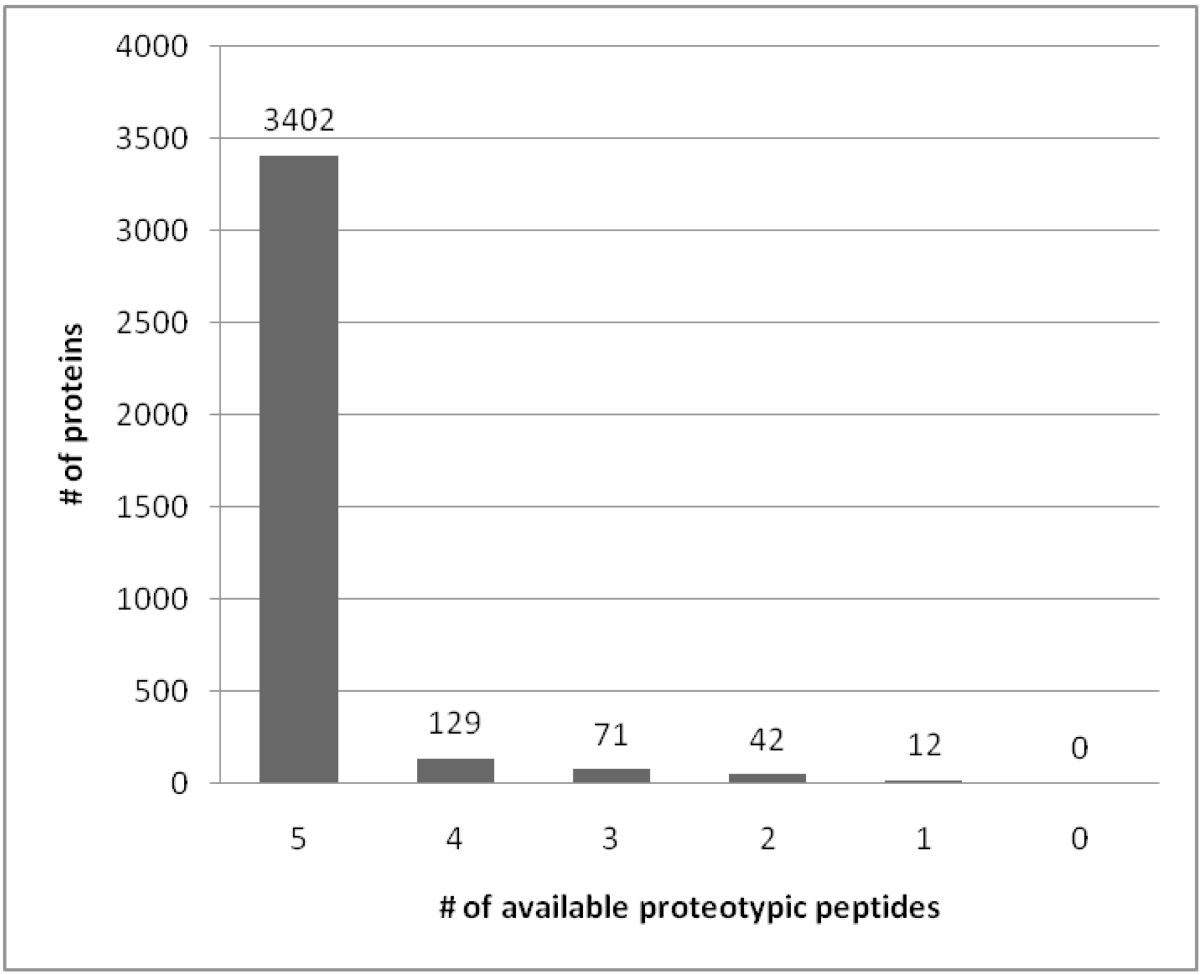

Figure S1. Accessibility of the *L. interrogans* proteome by LC-MS analysis. Number of proteins with their corresponding number of proteotypic peptides available for LC-MS/MS analysis after tryptic cleavage.

Figure S2:

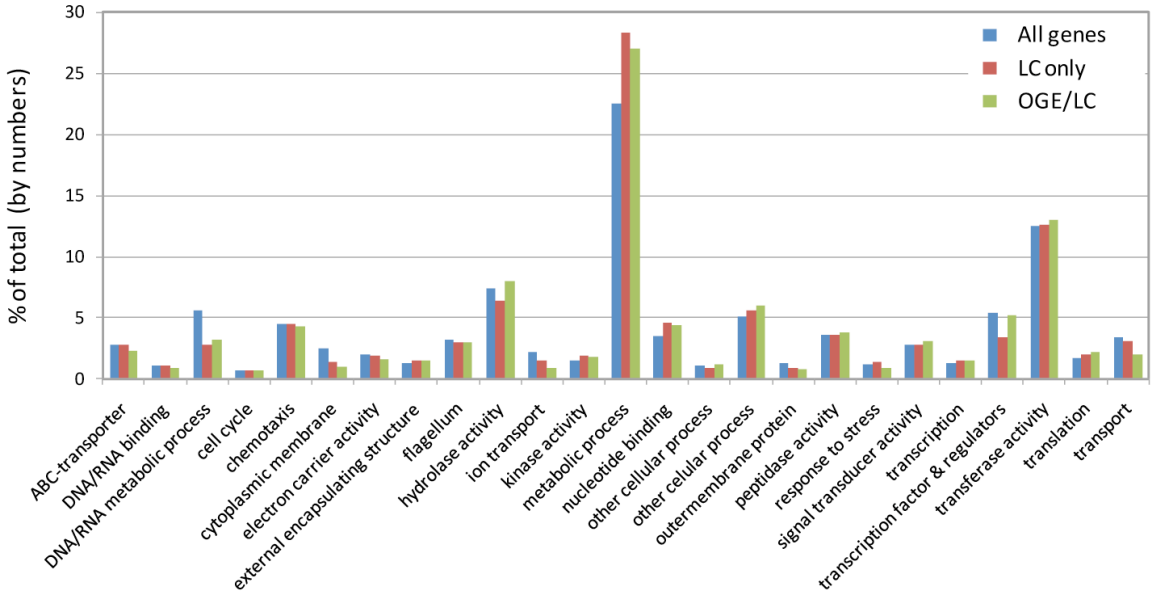

Figure S2. Functional annotation of the identified proteins. Distribution of the proteins identified by the LC-only (red) and OGE/LC (green) MS analysis in comparison to all predicted genes (blue) according to their functional categories as assigned by DAVID (Huang et al, 2007).

Figure S3:

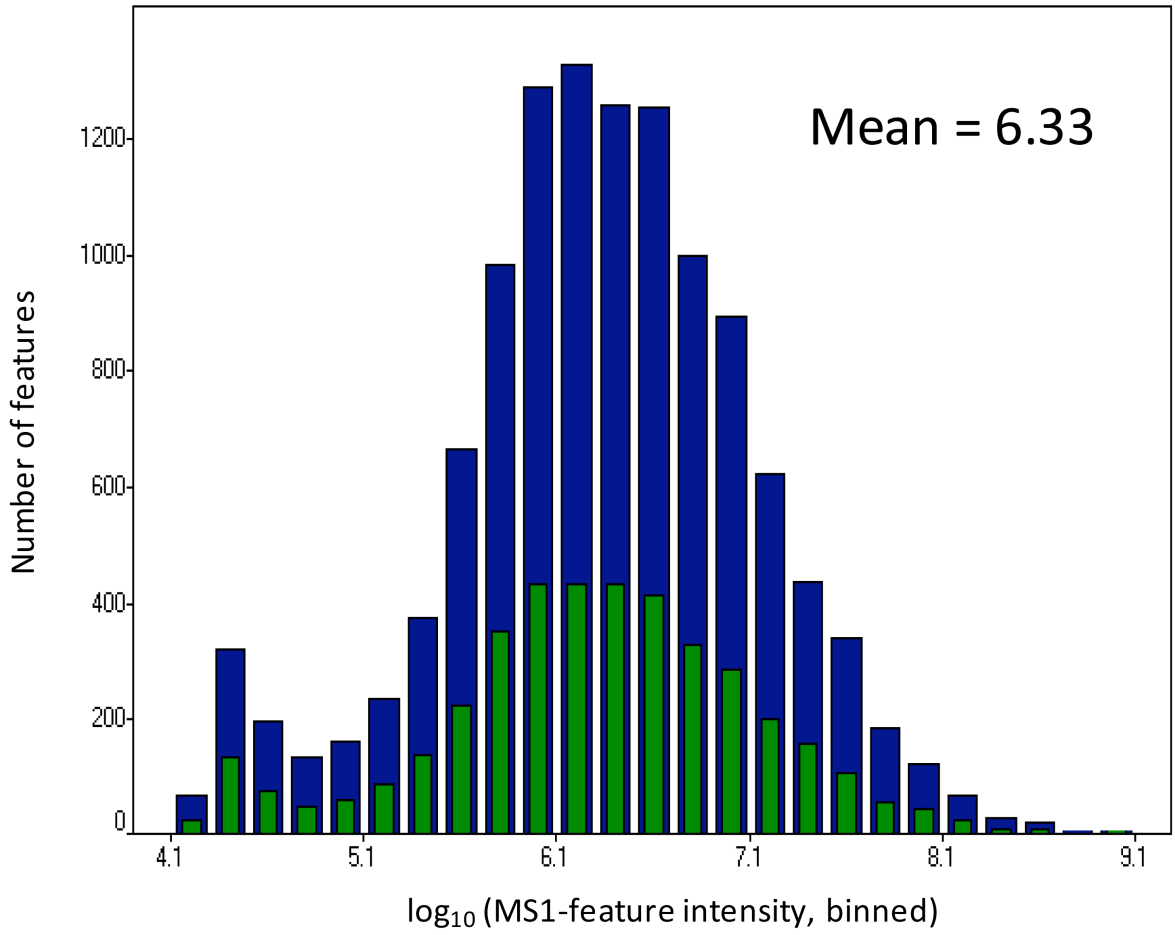

Figure S3. Distribution of MS1-feature intensities. Binned extracted precursor ion intensities (log_{10}) of all 13,113 features (blue) identified and the selected 4953 proteotypic peptides (green) for protein quantification.

Figure S4:

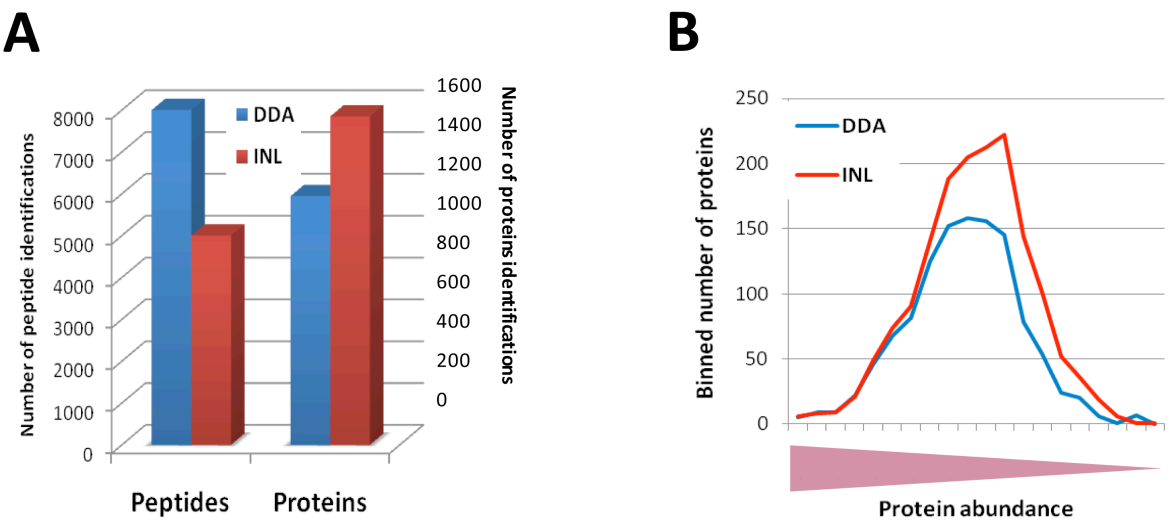

Figure S4. Comparison of the DDA- and directed (INL) LC-MS/MS strategy employed. (A) Analysis of the same peptide sample (control) with the same number of LC-MS/MS runs using either the data-dependent acquisition (DDA, blue) or the directed (INL, red) LC-MS/MS approach. The numbers of peptides and proteins identified by either approach are indicated. (B) Distribution of the proteins identified by the different approaches according to their abundance as determined by codon bias.

Figure S5:

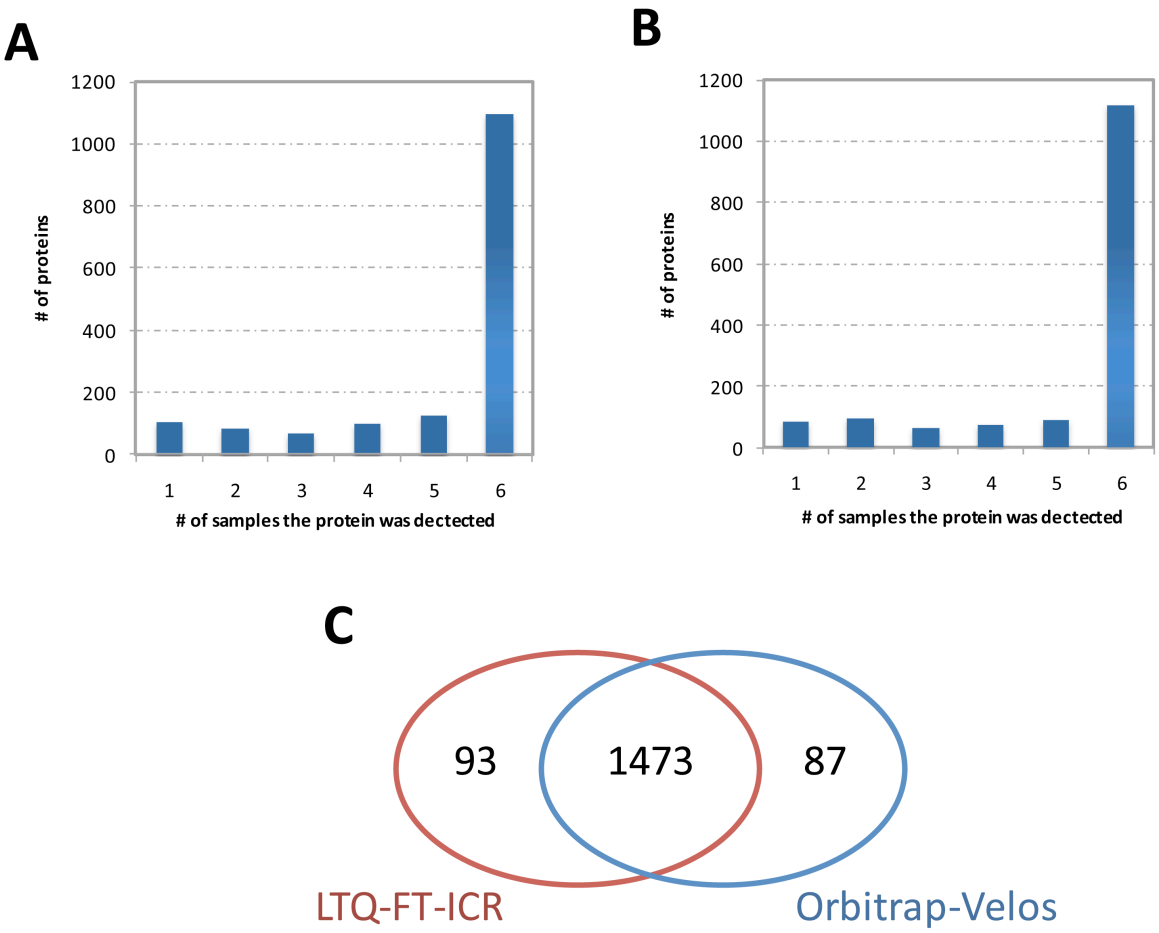

Figure S5. Performance of the directed MS-workflow using different LC-MS/MS platforms. (A) Number of times a protein was identified in 6 different control samples using directed mass spectrometry on the LTQ-FT-ICR LC-MS/MS platform. (B) Analysis of the same samples on a different LC (Proxeon Easy-LC) and MS (Orbitrap-Velos) system using the same peptide mass lists generated in the discovery phase. (C) Venn diagram showing the number of overlapping and specific protein fractions identified.

Figure S6:

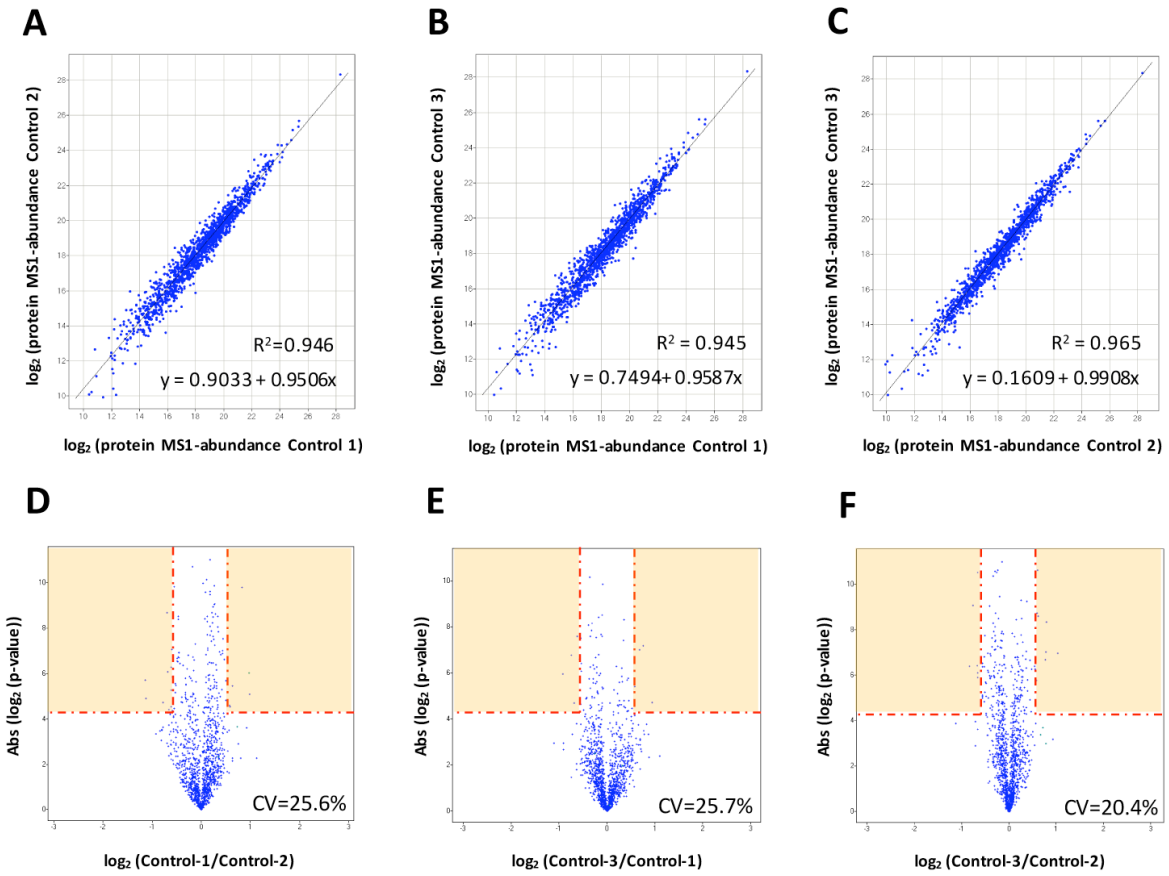

Figure S6. Reproducibility of label-free quantification of the *L. interrogans* proteome. (A-C) Scatterplots of protein MS-intensities (log_2) between various untreated replicate control samples as determined by the Progenesis software, including the respective squared Pearson correlation R^2. (D-F) Distribution of the protein ratios (log_2) determined from the same samples as indicated in A-C versus the significance value calculated from the ANOVA analysis. The coefficient of variance as well as the significant thresholds set for p-value (ANOVA, <0.05) and ratio (>1.5-fold) indicated as red lines are shown.

Figure S7:

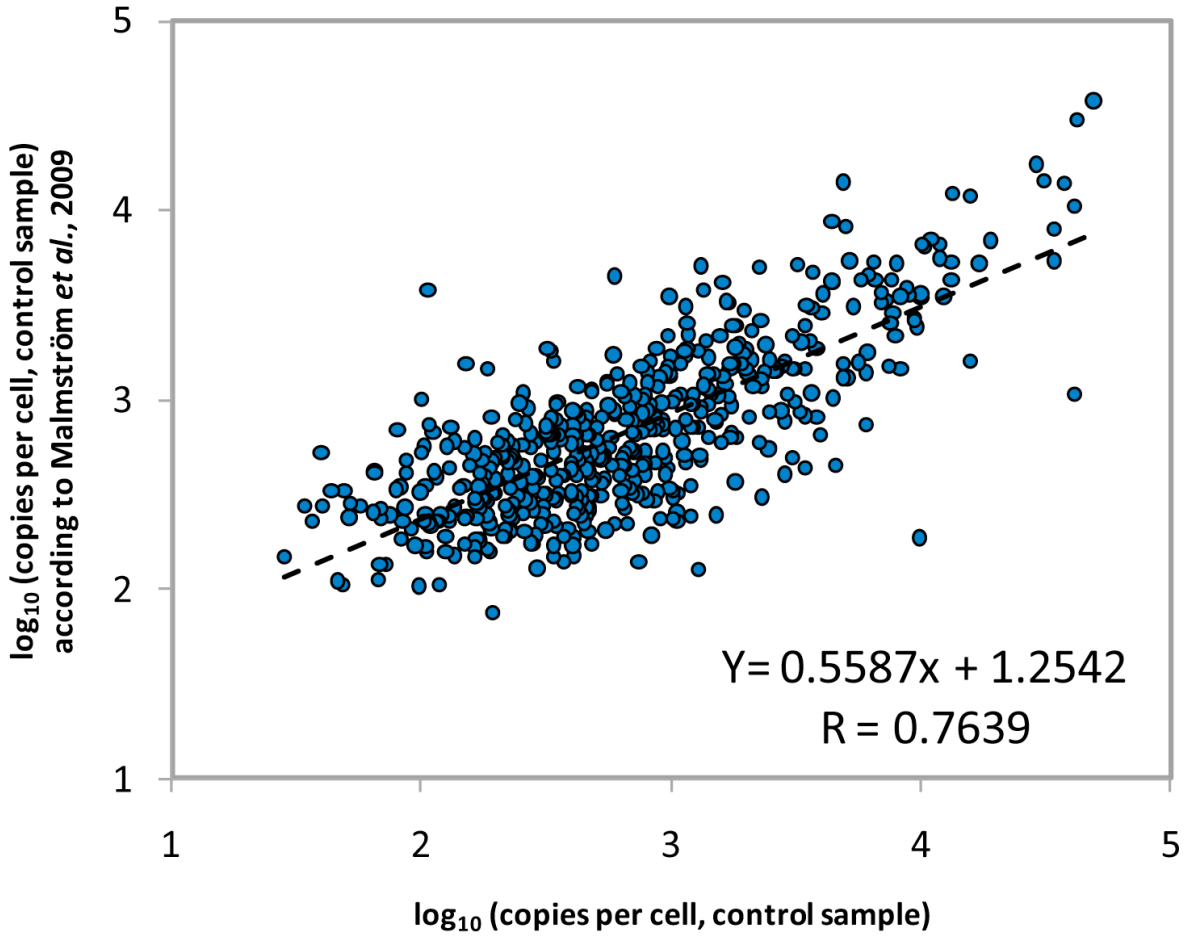

Figure S7. Correlation of the estimated protein abundances (in copies/cell) with a recently published study. Comparison of the protein abundances determined with a recently published dataset using a similar approach (Malmström et al, 2009).

Figure S8:

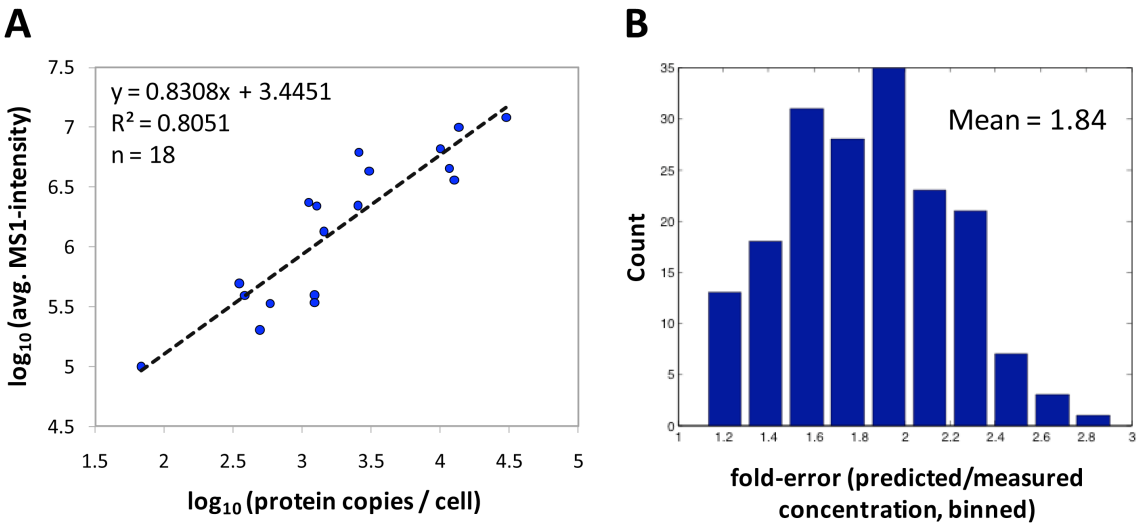

Figure S8. Determination of cellular protein concentrations. (A) Average extracted precursor ion intensities of the three most abundant peptides per protein (log_{10}) plotted against their protein concentration in copies/cell (log_{10}) determined using the spiked in heavy labeled reference peptides. (B) Distribution of fold-error rates calculated by bootstrapping according to (Malmström et al, 2009).

Figure S9:

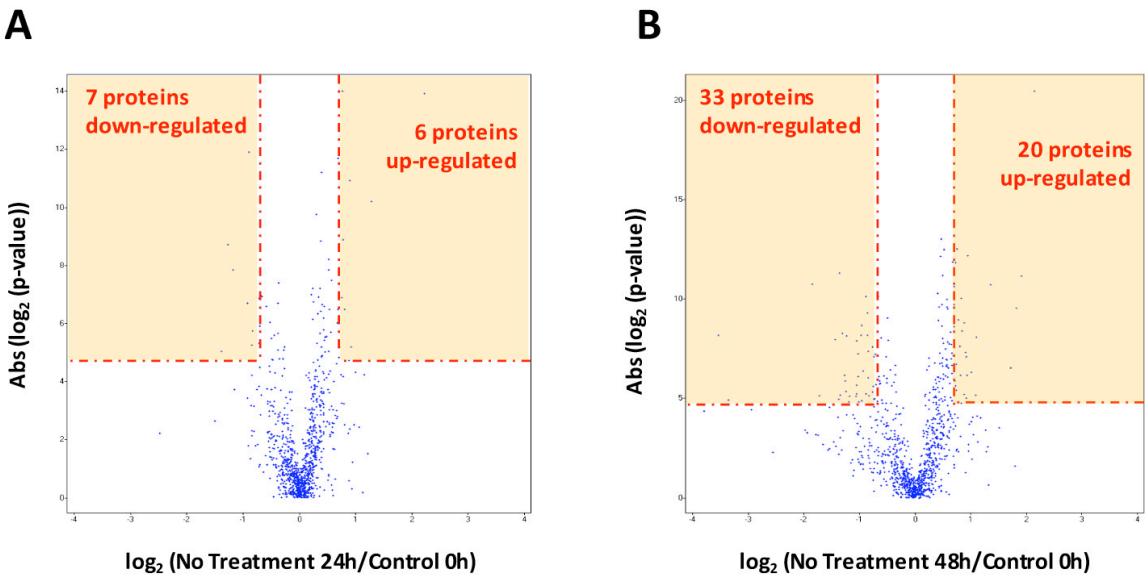

Figure S9. Significant protein changes detected in control samples. Volcano plots showing the significant protein abundance changes detected in control samples that were not subjected to any treatment after (A) 24 and (B) 48 hours. Protein regulations considered as significant ((ANOVA, <0.05) and ratio (>1.5-fold)) are indicated within the red lines together with the number of up- and down-regulated proteins.

Figure S10:

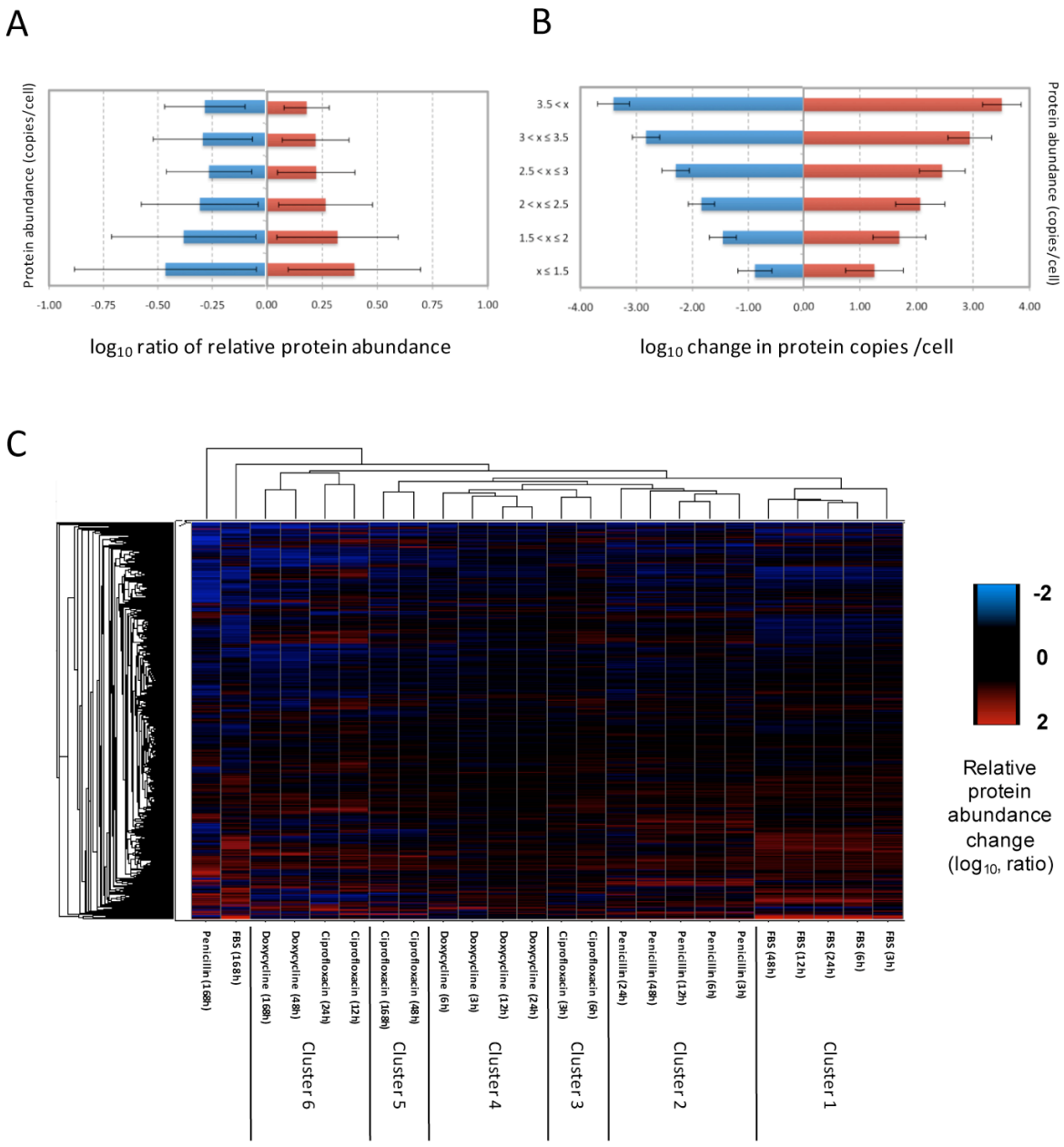

Figure S10. Impact of relative (in fold) and absolute (in copies/cell) protein level changes on the *L. interrogans* proteome. (A) Average relative abundance ratios (log_{10}) of all proteins grouped into 6 clusters of different concentration levels in the cell (control state). (B) Like A, using absolute protein concentration changes (log_{10}) instead fold-changes. The standard deviations calculated are indicated as error bars. (C) Hierarchical clustering of relative protein abundance changes (log_{10}) to the corresponding untreated control samples in copies per cell (log_{10}) for all 24 treatments. The column dendrogram representing the clustering of the differentially perturbed samples is displayed and the clusters (1-6) obtained are indicated.

Fig. S11:

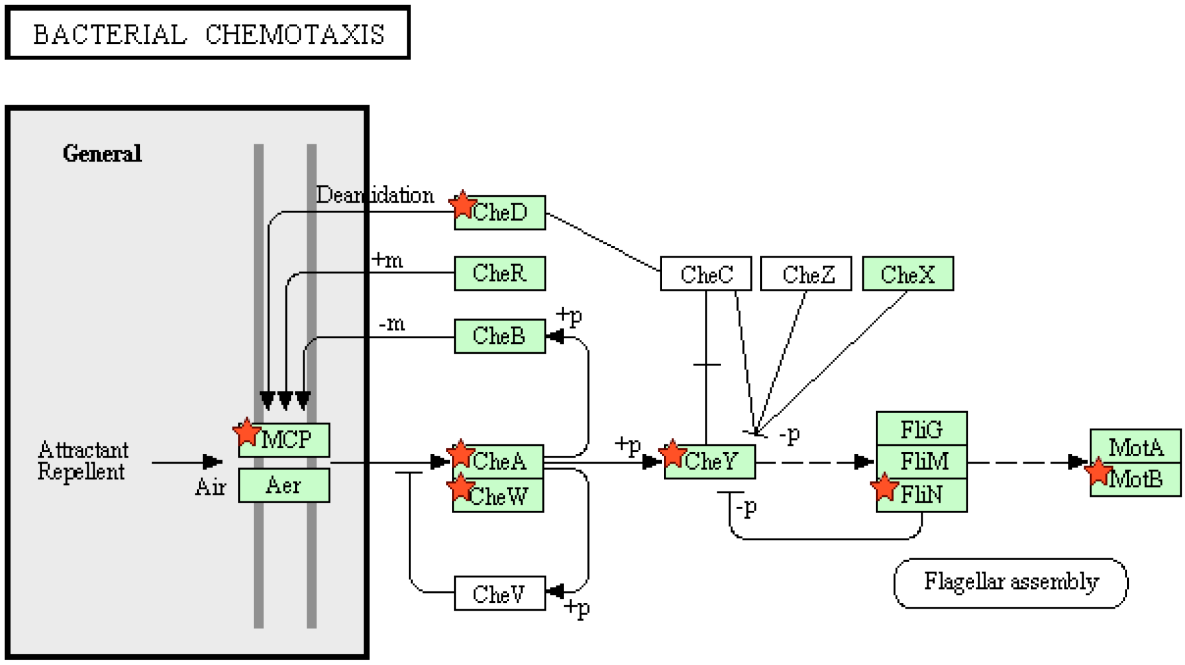

Figure S11. Proteins of the bacterial chemotaxis pathway covered in cluster S-5 as assigned by DAVID (Huang et al, 2007) using the KEGG database (Kanehisa et al, 2010). Proteins present in the cluster are indicated with a red star. Green (white) labeled genes are present (not present) in the *L. interrogans* genome.

Fig. S12:

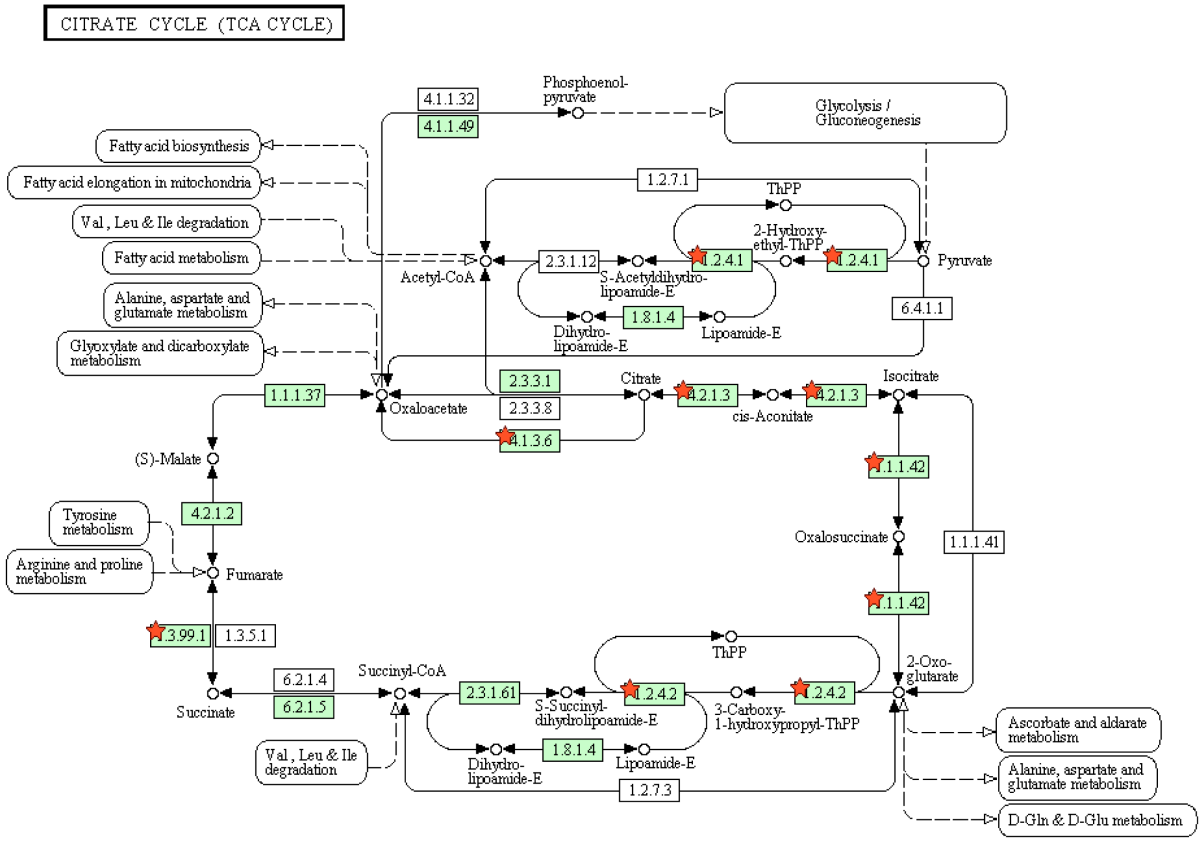

Figure S12. Proteins of the TCA cycle covered in cluster S-5 as assigned by DAVID (Huang et al, 2007) using the KEGG database (Kanehisa et al, 2010). Proteins present in the cluster are indicated with a red star. Green (white) labeled genes are present (not present) in the *L. interrogans* genome.

Fig. S13:

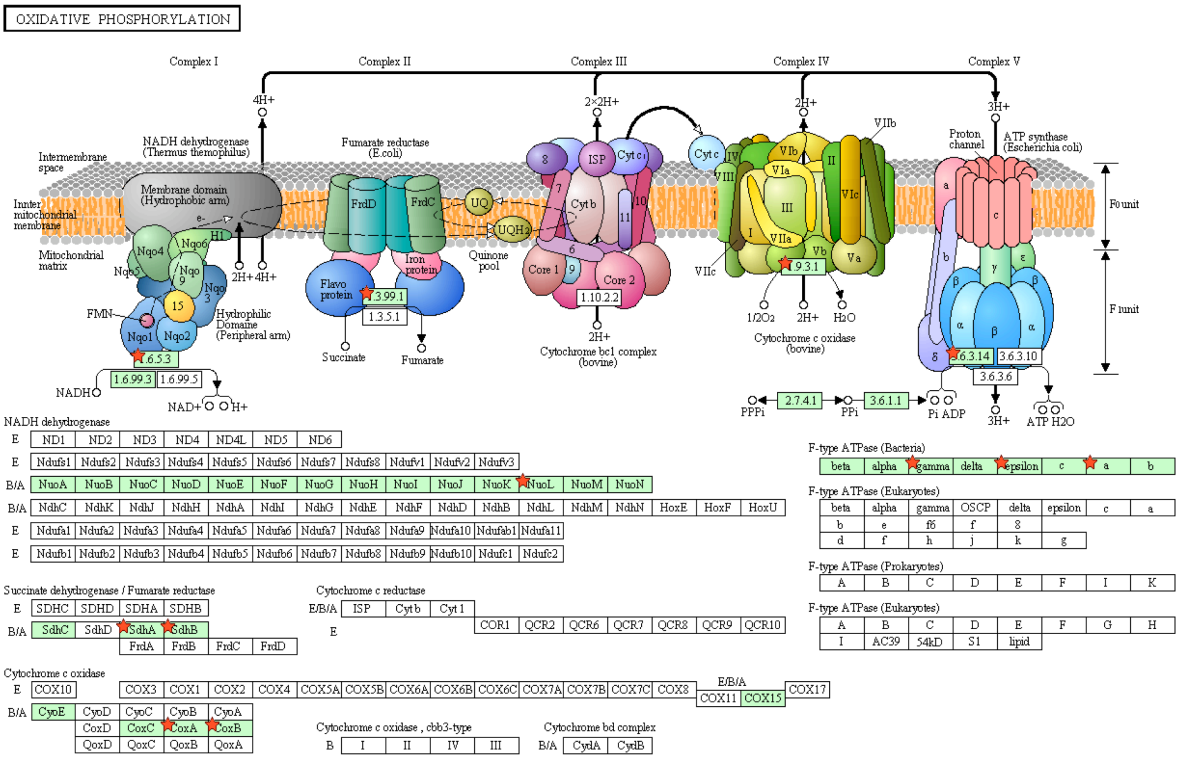

Figure S13. Proteins of the oxidative phosphorylation pathway covered in cluster S-5 as assigned by DAVID (Huang et al, 2007) using the KEGG database (Kanehisa et al, 2010). Proteins present in the cluster are indicated with a red star. Green (white) labeled genes are present (not present) in the *L. interrogans* genome.

Table SI. Protein abundance levels determined by stable isotope dilution LC-MS

Protein	Protein Name	Peptide Sequence	Peptide Copies/Cell[1]	Protein Copies/Cell[2]
gi|45656498|ref|YP_000584.1|	fatty acid synthase subunit beta	TEVITHANLVR	**1227**	**1227**
gi|45656647|ref|YP_000733.1|	DNA-directed RNA polymerase beta subunit	ITNLDYLPNLIQIQK	**1340**	**1280**
gi|45656647|ref|YP_000733.1|	DNA-directed RNA polymerase beta subunit	TFDLGEVGR	**1219**	
gi|45656648|ref|YP_000734.1|	DNA-directed RNA polymerase beta' subunit	FATSDLNDLYR	**1114**	**1114**
gi|45657072|ref|YP_001158.1|	flagellar hook protein	ENIGGVNPQQVGLGSLIAAIDK	**263**	**350**
gi|45657072|ref|YP_001158.1|	flagellar hook protein	VATAVFNNPAGLDK	**437**	
gi|45657124|ref|YP_001210.1|	ATP synthase subunit A	ILEVPVGPELLGR	**14,633**	**12,691**
gi|45657124|ref|YP_001210.1|	ATP synthase subunit A	TSIALDTILNQK	**10,749**	
gi|45657126|ref|YP_001212.1|	ATP synthase subunit B	FSQAGSEVSALLGR	**10,042**	**10,042**
gi|45657141|ref|YP_001227.1|	MreB	GIVLTGGGCLLR	**3205**	**3063**
gi|45657141|ref|YP_001227.1|	MreB	TGGDEFDEAIIK	**2921**	
gi|45657213|ref|YP_001299.1|	GroEL	AVTAAVESIQK	**10,572**	**13,649**
gi|45657213|ref|YP_001299.1|	GroEL	VEDALSATR	**16,726**	
gi|45657214|ref|YP_001300.1|	GroES	ESDILAVVK	**13,686**	**11,704**
gi|45657214|ref|YP_001300.1|	GroES	VGDTVLYGK	**9723**	
gi|45657269|ref|YP_001355.1|	flagellar M-ring protein	GFTPDGPAGTEPNIAPGYK	**75**	**68**
gi|45657269|ref|YP_001355.1|	flagellar M-ring protein	IISDFEEDLEK	**60**	
gi|45657473|ref|YP_001559.1|	ATP-dependent protease ATP-binding subunit	LLEEVSFEGPDLPESQR	**1227**	**1227**
gi|45657611|ref|YP_001697.1|	recombinase A	IVEIYGPESSGK	**384**	**384**
gi|45657810|ref|YP_001896.1|	ATP-dependent CLP protease-like, proteolytic subunit	IAEVFEELTGSK	**2337**	**2585**
gi|45657810|ref|YP_001896.1|	ATP-dependent CLP protease-like, proteolytic subunit	IFLWGPVTDESSK	**1401**	
gi|45657810|ref|YP_001896.1|	ATP-dependent CLP protease-like, proteolytic subunit	LNQILADACGHPISK	**4015**	
gi|45657869|ref|YP_001955.1|	ATP-dependent protease	AVDLIDEASSK	**550**	**493**
gi|45657869|ref|YP_001955.1|	ATP-dependent protease	IADIQLEGLR	**437**	
gi|45657961|ref|YP_002047.1|	30S ribosomal protein S6	EFLINQNILR	**4961**	**4961**
gi|45658059|ref|YP_002145.1|	Hsp15-like protein	ILELPTEVDSEK	**813**	**813**
gi|45658060|ref|YP_002146.1|	Hsp15	DVQVQLEK	**587**	**587**
gi|45658686|ref|YP_002772.1|	30S ribosomal protein S5	FSFNALSVVGDQR	**2529**	**2529**
gi|45659137|ref|YP_003223.1|	fatty acid synthase subunit beta	EFFDTSFK	**1445**	**1445**

1) Endogenous peptide abundances determined by stable isotope dilution
2) If multiple peptides per protein were identified and quantified, the average abundance level is shown